Determining the dominant degradation mechanisms in Nitrocellulose

Amy J. Lai

A thesis submitted in partial fulfilment

of the requirements for the degree of

Doctor of Philosophy

of

University College London.

Department of Chemistry

University College London

February 7, 2020

Declaration

I, Amy Lai , confirm that the work presented in this thesis is my own. Where information has been derived from other sources, I confirm that this has been indicated in the work.

Abstract

The dominant degradation pathways of nitrocellulose (NC) were investigated, using quantum mechanics (QM) methods to probe the primary denitration routes, followed by key secondary reactions. The polymer structure was truncated in order to facilitate density functional theory (DFT) studies into the mechanistic details of denitration at individuate nitrate sites. Comparison of monomer, dimer and trimer units of the polymer using quantum theory of atoms in molecules (QTAIM) topology analysis of interaction sites, analysis of the electrostatic potential (ESP) and charges showed that the most suitable model for study of the decomposition reactions was β-glucopyranose monomer, bi-capped with methoxy groups. The model was nitrated at the C2 position, to mimic the most stable nitration site [1]. The primary thermolytic and hydrolytic denitration routes were explored using transition state (TS) searches and potential energy surface (PES) scans. It was found that the thermolytic behaviour of the NC denitration step matched the energy profile of other nitrate esters [2]. Protonation at the bridging oxygen site of the nitrate was found to be the most likely to lead to denitration. It was not possible to isolate a TS for the hydrolytic reaction, though a number of coordination schemes were tested. Secondary processes following initial denitration were examined. Ethyl nitrate was used as a test system before extension to the monomer. Different reaction pathways for decomposition, with forward propagation of the evolved species to the reaction step, revealed that $^{\cdot}NO_2$ was the most likely cause for the experimentally observed autocatalytic rate of degradation.

Impact Statement

This study examines the degradation properties of NC, shedding light on the mechanistic details of decomposition that are yet currently either unknown, or are unclear in existing literature. NC is used in an extensive variety of products, with utilisation in household, industrial, military and medicinal applications. Improved understanding of the fundamental chemistry in the degradation of NC could benefit the following key impact areas:

Knowledge & collective benefit

- Broaden understanding and depth of knowledge in the area of NC degradation, with the view to validate or deconflict competing schemes in literature.
- Improve conservation practices for existing and legacy NC products of cultural value, such as cinematographic film, artworks and historical munitions with better information on environmental conditions most impacting the decomposition pathways.

Environmental

- Inform improved NC disposal methods, avoiding existing harsh chemical and incineration treatments, with opportunity to feed back into other manufacture streams such as the production of fertiliser.
- Facilitate the design of next generation NC products with lower environmental impact, in terms of durability and recycle-ability, with cleaner industrial processes.

Safety

- Refine guidelines on safety and usage, based on detailed knowledge of the degradation mechanisms, improving upon current practices based on aggregate experimental observations.

Industrial & commercial

- Improve versatility and adaptability in NC production and its product formulations, in view of varying cellulose feedstock sources due to supply chain fluctuation.
- Streamline industrial processes to specific reactivity requirements, based on detailed mechanistic considerations regarding shelf life and interaction with other components, leading to cost saving and better performance of final product.

Innovation

- Allow the design of new NC products, not limited by crude understanding about the material shelf life and reactivity, leading to novel applications.

Contents

List of Figures

List of Tables

Abbreviations

%N	percentage nitrogen by mass
2-NDPA	2-Nitrodiphenylamine
AIMD	*ab initio* molecular dynamics
AO	atomic orbital
a.u.	atomic units
B3LYP	Becke, 3-parameter, Lee-Yang-Parr hybrid functional
BCP	bonding critical point
BSSE	basis set superposition error
CH_3CH_3	NC repeat unit with two $-OCH_3$ capping groups
CH_3OH	NC repeat unit with $-OCH_3$ capping group on ring 1 and $-OH$ group on ring 2
CCP	cage critical point
CP	critical point
DFT	density functional theory
DFT-D	density functional theory with dispersion correction
DSC	differential scanning calorimetry
DOS	degree of substitution
DPA	diphenylamine

EM energetic materials

EN ethyl nitrate

ESP electrostatic potential

G09 Gaussian 09 revision D.01

GGA generalised gradient approximation

GM genetically modified

GTO Gaussian type orbitals

GView Gauss View 5.0.8

HF Hartree-Fock

HMF hydroxymethylfurfural

HOMO highest occupied molecular orbital

IR infra-red spectroscopy

KS-DFT Kohn-Sham DFT

LDA local density approximation

MD molecular dynamics

MEP minimum energy path

MM molecular mechanics

MMFF94 Merck molecular force field 94

MO molecular orbitals

MP2 Møller–Plesset perturbation theory with second order correction

MW molecular weight

NBO natural bond orbital

NC nitrocellulose

NCP nuclear critical point

NG nitroglycerine

NMR nuclear magnetic resonance spectroscopy

$OHCH_3$ NC repeat unit with $-$OH capping group on ring 1 and $-OCH_3$ group on ring 2

PCM polarisable continuum model

PES potential energy surface

PETN pentaerythritol tetranitrate

PETRIN pentaerythritol trinitrate

QM quantum mechanics

QTAIM quantum theory of atoms in molecules

RCP ring critical point

RESP restrained electrostatic potential atomic partial charges

RHF restricted HF

ROHF restricted-open HF

UHF unrestricted HF

SB59 1,4-bis(ethylamino)-9,10-anthraquinone dye

SCF self-consistent field

SEM scanning electron microscopy

SMD solvation model based on density

S_N2 bi-molecular nucleophilic substitution reaction

STO Slater type orbitals

TG thermogravitmetric analysis

TS transition state

UFF universal force field

UV ultraviolet

UVvis ultraviolet–visible spectroscopy

vdW van der Waals

ωB97X-D ωB97X-D long-range corrected hybrid functional

ZPE zero-point energy

Chapter 1

Post-Denitration Reactions

1.1 Introduction

Products of the preliminary denitration step of NC can be evolved as gases or remain trapped in the polymer matrix. Reactive nitrogen dioxide radicals generated from homolysis of the O-N bond are likely to migrate within the bulk and attack other sites on the polysaccharide, initiating branched radical chain reactions. These lead to deeper decomposition of the polymer *via* chain scission and rupture of glucose rings, with eventual complete disintegration of the molecule, assisted by products released by ongoing acid hydrolysis. Nitrous and nitric acids are released directly from denitration or via transformation of released NO_x species. In addition to catalysing hydrolysis, they increase the acidity of the overall system, lowering the pH and stimulating further hydrolytic processes [7]. The final product mixture is dictated by the numerous side reactions involving autocatalysis, radical reactions and product interactions.

When studying the ageing of NC using UVvis spectroscopy, Moniruzzaman *et al.* observed increasing concentrations of reaction products beyond those generated from first-stage decomposition, following heat treatment over extended timescales [8, 3]. The reaction of the SB59 with NO_x released by denitration, mimics the action of stabilisers such as diphenylamine (DPA) and 2-Nitrodiphenylamine (2-NDPA) commonly used in NC formulations. The secondary amine groups of the dye consume any nitrates in the system, eliminating the possibility of successive reactions generating acidic species. Un-aged NC thin films, and films aged at 40°C, 50°C, 60°C and 70°C for timescales of up to 2000hrs for 40°C, were compared. UV absorbances at 600 nm and 650 nm were characteristic of the SB59 dye used to indicate the presence of NO_x, released by the denitration of NC (figure 1.2). The isosbestic point identified at 552 nm showed a proportional relationship

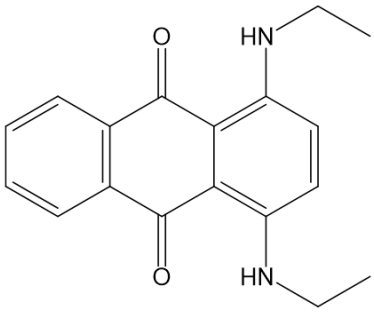

Figure 1.1: 1,4-bis(ethylamino)-9,10-anthraquinone dye (SB59) used to probe the release of nitrates from NC using UVvis and ^{1}H NMR spectroscopy [3]. The action of nitrate absorption by the dye imitates that of stabilisers commonly used with nitrate ester formulations.

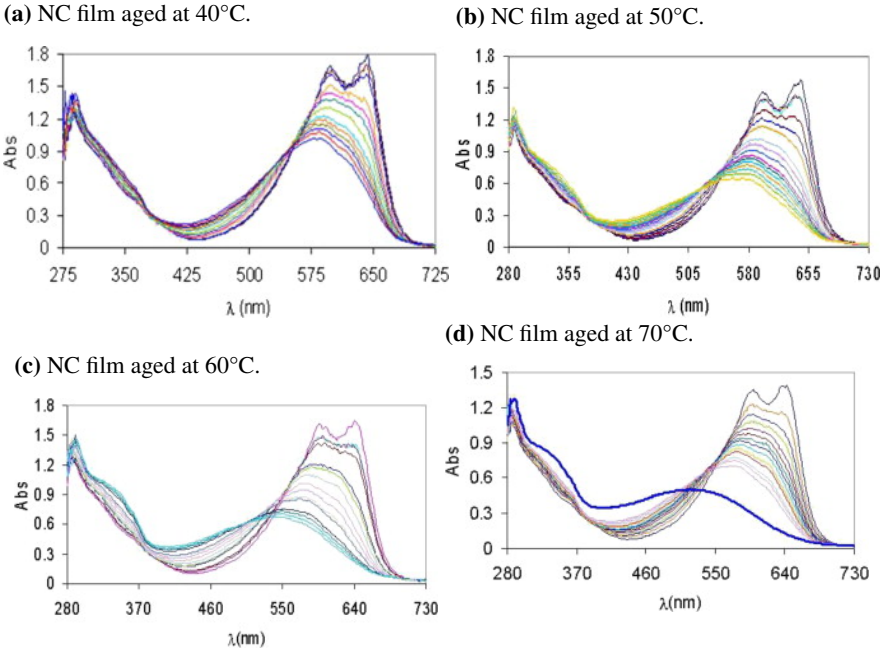

Figure 1.2: UVvis spectra of aged NC-based film, from the work of Moniruzzaman *et al.*[3]. The peaks at 600 nm and 650 nm are attributed to the π - π* transitions in the anthraquinone dye (SB59). Spectral lines with highest absorbance peaks in this region correspond to the sample prior to heat treatment. Peaks below 400 nm indicate the formation of SB59 derivatives due to secondary reactions.

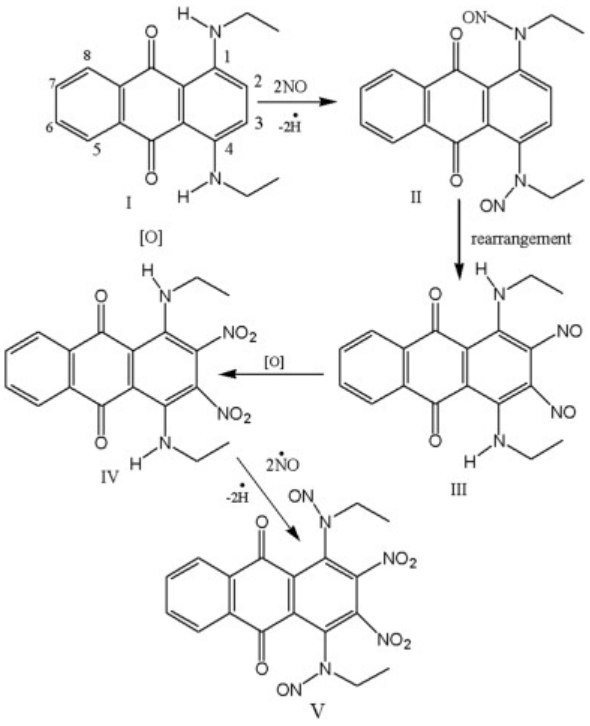

Figure 1.3: Proposed pathway for the reaction of SB59 dye with ·NO released as a result of denitration of NC [3].

between the concentration of SB59 as it decreased, with the concentration of the [SB59 + NC] product as it increased. Samples exposed to higher ageing temperatures presented spectra dominated by products formed *via* secondary reactions. For samples aged at temperatures >40°C, the isosbestic point demonstrated a downwards shift with increasing dye consumption. In the case of the 70°C treated run, the final measurement (indicated by the royal-blue line in bold in figure 1.2d)) deviated from the isosbestic point entirely, with more than 81% consumption of the original dye concentration. The drift from the isosbestic point, in addition to the appearance of new absorbance peaks below 400 nm, allude to the presence of new species in the reaction mixture not generated by the primary reaction of SB59 and NC. It is likely that these arise from the continued reaction of SB59 derivatives with NC degradation products, or further derivatives thereof, as suggested in figure 1.3. Following cleavage of the nitrate ester via homolytic fission, elimination of nitrous acid, or hydrolysis, the resulting residues available for further reaction with the polymer or other free molecules in the system. In the study of pentaerythritol tetranitrate (PETN) ageing at high temperatures (115°C - 135°C) in vacuum, and low temperatures (20°C - 65°C) in acetonitrile solution, Shepodd *et al.* commented that thermolysis produced a more complex and varied mixture, due to deeper degradation and recombination of radicals [9]. By

Scheme 1.1: Thermolytic initiation

$$R{-}ONO_2 \longrightarrow R{-}O^{\cdot} + {}^{\cdot}NO_2 \tag{1.1}$$

Propagation

$$R{-}O^{\cdot} + {}^{\cdot}NO_2 \xrightarrow{R{-}ONO_2} R{-}ONO_2 + {}^{\cdot}NO + {}^{\cdot}NO_2 + N_2O_4 + H_2O + N_2O + CO_2 + CO + C_2H_2O + \text{other organic fragments} \tag{1.2}$$

$$2\,{}^{\cdot}NO + O_2 \longrightarrow 2\,{}^{\cdot}NO_2 \tag{1.3}$$

$$2\,{}^{\cdot}NO_2 \rightleftharpoons N_2O_4 \tag{1.4}$$

Scheme 1.2: Hydrolytic initiation

$$R{-}ONO_2 + H_2O \longrightarrow R{-}OH + HNO_3 \tag{1.5}$$

$$R{-}OH + HNO_3 \longrightarrow R{=}O + HNO_2 + H_2O \tag{1.6}$$

Propagation

$$HNO_3 + HNO_2 \rightleftharpoons N_2O_4 + H_2O \tag{1.7}$$

$$N_2O_4 \rightleftharpoons 2\,{}^{\cdot}NO_2 \tag{1.8}$$

$$R{-}OH + {}^{\cdot}NO_2 \longrightarrow {}^{\cdot}R{-}OH + HNO_2 \tag{1.9}$$

$${}^{\cdot}R{-}OH + HNO_3 \longrightarrow R{=}O + H_2O + {}^{\cdot}NO_2 \tag{1.10}$$

contrast, the low temperature hydrolytic process emphasised formation of pentaerythritol trinitrate (PETRIN) followed by side reactions with reduced likelihood of radical recombination in solution compared to in a solid, as ${}^{\cdot}NO_2$ would be more likely to diffuse and react elsewhere. Chin *et al.* proposed schemes for the propagation of secondary reactions initated by both the thermolysis (scheme 1.1) and hydrolysis of nitrate esters (scheme 1.2) [5].

Termination reactions were not emphasised in either of the schemes for these cases. The hydrolysis scheme was adapted from an earlier work by Camera *et al.* involving the nitrate

Scheme 1.3: Hydrolysis scheme for ethyl nitrate

$$CH_3CH_2ONO_2 + H^+ \overset{\text{fast}}{\rightleftharpoons} CH_3CH_2ONO_2H^+ \tag{1.11}$$

$$CH_3CH_2ONO_2H^+ \overset{\text{slow}}{\rightleftharpoons} CH_3CH_2OH + {NO_2}^+ \tag{1.12}$$

$${NO_2}^+ + 2\,H_2O \overset{\text{fast}}{\rightleftharpoons} HNO_3 + H_3O^+ \tag{1.13}$$

ester decomposition and subsequent reactions of EN (where R = CH_3CH_2 for the scheme above) [4]. The original study included an expansion of the hydrolysis step (equation 1.11), where the involvement of NO_2^+ was illustrated (scheme 1.3).

It was highlighted by Camera, that the oxidation of alcohol by nitric acid (equation 1.6) is slow and thus rate-limiting. The mechanism is likely to occur *via* a series of intermediate reactions of which the details are not known. Following the generation of nitrous acid, subsequent oxidations occur rapidly. According to Rigas *et al.*, alcohols are more susceptible to wet oxidation than esters [10]. A higher concentration of unsubstituted hydroxyl groups in the system, and therefore a fewer nitrate ester groups (or a lower degree of substitution (DOS) value), decreases overall stabililty.

Equations 1.7 - 1.10 describe a possible branched radical chain mechanism, fed by the nitrous and nitric acids produced during the hydrolysis and alchohol oxidation reactions during the initiation stage. By contrast, the propagation reactions in the branched radical chain mechanism for thermolysis are poorly characterised (equation 1.2), defined only by the observable products. This is likely due to their rapid and varied nature, rendering it difficult to follow spectroscopically.

Aellig *et al.* presented an alternative scheme for the decomposition of benzyl nitrate (R = $PhCH_2$), involving more interaction with the solvent [6]:

Both the Camera/Chin and Aellig schemes above produce final end products observed in

Scheme 1.4: HNO_3 decomposition initiation

$$4\,HNO_3 \rightleftharpoons 4\,^{\cdot}NO_2 + 2\,H_2O + O_2 \tag{1.14}$$

$$2\,^{\cdot}NO_2 + H_2O \rightleftharpoons N_2O_4 + H_2O \tag{1.15}$$

$$N_2O_4 + H_2O \longrightarrow HNO_3 + HNO_2 \tag{1.16}$$

Propagation

$$R{-}OH + HNO_2 \rightleftharpoons R{-}ONO + H_2O \tag{1.17}$$

$$R{-}ONO \longrightarrow R{=}O + HNO \tag{1.18}$$

$$^{\cdot}NO_2 + HNO \longrightarrow HNO_2 + {}^{\cdot}NO \tag{1.19}$$

$$2\,^{\cdot}NO + O_2 \longrightarrow 2\,^{\cdot}NO_2 \tag{1.20}$$

Termination

$$2\,HNO \longrightarrow HON{=}NOH \tag{1.21}$$

$$HON{=}NOH \longrightarrow N_2O + H_2O \tag{1.22}$$

the decomposition of NC. In particular, Aellig's scheme accounts for the production of N_2O, which forms a significant part of the decomposition eluent [11]. Whilst the schemes do not a propose an exhaustive description of the full spectrum of reactions that take place in the NC matrix during its slow ageing, the early stage reactions of the key species responsible for decomposition are encapsulated.

It is widely agreed that first-stage decomposition follows a first-order process (or pseudo-first order, with respect to hydrolysis reactions). A number of studies observe catalytic rate of decay for the longer-term aging processes. Dauerman [12] observed that when NC was treated with NO_2 gas before heating, the time required for sample ignition halved. He suggested that the NO_2 adsorbed onto the surface acted as a catalysing agent.

Neutral and alkaline hydrolysis reactions follow a pseudo-first order process, however it has been suggested that the presence of acid facilitates a catalytic rate of degradation after an initial incubation period. Multiple studies have addressed the decomposition reactions of nitrate esters following the initial scission of the nitrate group [13, 4, 14, 15, 7] In their work looking into the atmospheric reactions of methynitrate and methylperoxy nitrate Arenas suggested it was possible for the homolytic denitration reaction of methynitrate to share a common peroxy intermediate with the peroxide [16]. This could account for some of the lower order NO_x generated. In this section, secondary and extended reaction schemes for the low temperature ageing of NC are explored. Decomposition pathways defined by Chin, Camera and Aellig *et al.* are probed to determine the reactions responsible for the experimentally observed degradation products. The reactions found to be energetically feasible from the proposed routes will be scrutinised to determine whether an autocatalytic pathway can be formed from the thermodynamically validated reaction schemes.

1.2 Methodology

The schemes proposed by Chin, Camera and Aellig *et al.* were used to construct possible degradation routes for NC with the products of homolytic fission, elimination of HNO_2 and acid hydrolysis used as the starting point. Pathways were constructed based on propagation of the given reactions in a step-wise fashion; subsequent reactions were dependent on the products generated in preceding steps. An abundance of water and oxygen were assumed present in the system, attributed to air exposure under the wetted storage conditions of NC. Unsubsitutued alcohol moieties (R-OH) were also presumed available, due to incomplete nitration during the synthesis of NC [17], and re-generation following denitration *via* hy-

drolysis. The schemes were modelled with EN, then expanded to the NC monomer. Free energies of reaction (Δ G) were used to determine the feasibility of each reaction.

1.2.1 Computational details

All geometry optimisations were conducted in Gaussian 09 revision D.01 (G09), using the ωB97X-D and B3LYP functionals. Optimisations and thermochemistry calculations were performed to the level of 6-31+G(2df,p) with tight convergence criteria (table **??**). Calculations were performed in both vacuum and with polarisable continuum model (PCM) to introduce implicit solvent effects. Chemical species were constructed using Gauss View 5.0.8 (GView) and for molecules of more than 3 atoms, the "Clean" function was used to re-order atoms to a preliminary starting geometry. Energies of optimised structures were checked against values listed on NIST Computational Chemistry Comparison and Benchmark Database [18] if analogous molecules to a similar level of theory were available.

1.3 Results and Discussion

Simplified schemes for the possible ageing reactions of nitrate esters beginning from homolytic fission, elimination of HNO_2 or acid hydrolysis are illustrated in schemes 1.5 - 1.7. When starting with the products of homolytic fission, a branched radical chain mechanism dominates. $^{\cdot}NO_2$ and HNO_2 were consumed and regenerated, supporting the theory that these may be species contributing to the observed autocatalytic rate of decomposition, following a first-order rate induction period [19, 20, 21]. For all schemes, R=O and N_2O were terminating species. Whilst $N_2O$is released into the environment, R=O remains in the system may go on to participate in further decomposition reactions leading to ring opening. The protonation site of EN was inspected to determine whether it matched that of the hydrolytic denitration of NC, therefore following the same extended hydrolysis scheme.

Table 1.1: Free energies of protonation for each oxygen site on EN.

Protonated site		ΔG_r /kCal mol^{-1}			
		ωB97X-D	PCM	B3LYP	PCM
Terminal (upper)	$CH_3CH_3ONO_2H^+$	−12.28	8.82	−13.78	5.63
Terminal (lower)	$CH_3CH_3ONO_2H^+$	−9.48	9.46	−11.13	5.65
Bridging	$CH_3CH_3O(H^+)NO_2$	−9.32	9.06	−15.31	6.67

Table 1.1 shows the protonation energies for the three different oxygen sites on EN. Despite the upper terminal oxygen possessing the most thermodynamically favourable en-

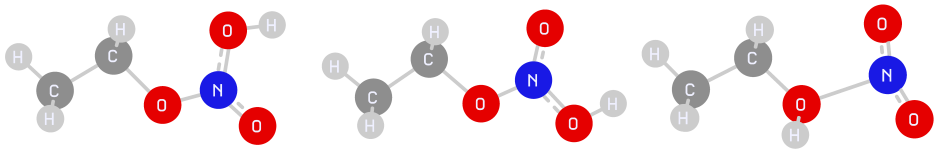

(a) Upper terminal oxgen. Bond(O–NO_2): 1.28 Å

(b) Lower terminal oxgen. Bond(O–NO_2): 1.28 Å

(c) Bridging oxgen. Bond(O–NO_2): 1.98 Å

Figure 1.4: Optimised geometries of the possible protonation sites on EN.

ergy of protonation, inspection of the reaction geometries shows that the bridging structure most resembles that expected for the liberation of the NO_2^+ group at the next step. Though appearing less thermodynamically favourable when compared to protonation at the terminal upper oxygen site, the higher energy of reaction likely arises from the instability of the protonated complex. The elongation of the $O-NO_2$ bond allows stabilisation of the proton at the bridging site, faciliting the facile departure of NO_2^+. Subsequent calculations involving the energy of the protonated EN will employ the values associated with the protonated bridging site.

Table 1.2 shows the energies for the reactions in all schemes, for both EN and the NC monomer.

The ωB97X-D long-range corrected hybrid functional (ωB97X-D) values obtained for the formation of N_2O_4 from $2^{\cdot}NO_2$ are in good agreement with the experimentally recorded value of -1.4 kCal mol^{-1} [22, 23]. It is noted that the Becke, 3-parameter, Lee-Yang-Parr hybrid functional (B3LYP) result does not perform so well for this reaction. This may arise from a number of factors, including the limitation to short-range interactions in B3LYP, or the geometry optimisation procedure, whereby a small variation or imperfect minimisation in the obtained optimised structures for the reaction species is amplified in the calculation of reation energies. Comparison of reaction energies for EN and the monomer shows that most processes are more thermodynamically favourable in the case of NC.

1.4 Summary

A number of proposed reactions following the denitration of NC were validated by calculating energies of reaction with the ωB97X-D and B3LYP methods.It as found that except in the case nitric acid decomposition, $4\,HNO_3 \rightleftharpoons 4\,NO_2 + 2\,H_2O + O_2$, most reactions were feasible at atmospheric conditions. The reactions were used to create rough schemes of the possible routes degradation routes, with increasing number of the NC decay. It can be seen

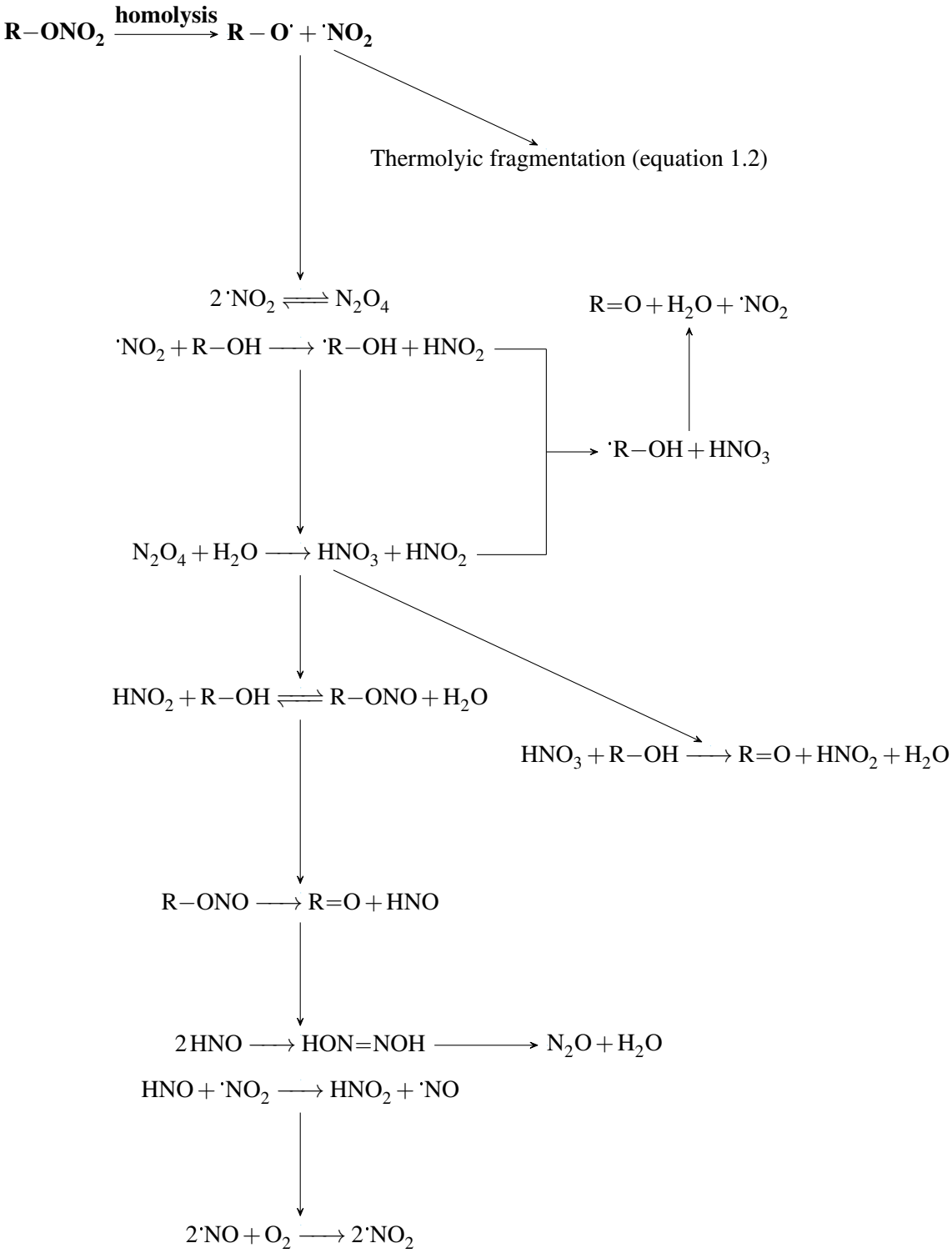

Scheme 1.5: Proposed degradation pathway starting from the homolytic fission of the nitrate ester, derived from the schemes presented by Camera [4] and Aellig[6].

Table 1.2: Energies of nitrate ester decomposition reactions proposed by Camera [4], Chin [5] and Aellig [6]. R = CH_3CH_2 for EN, and R = $(H_3CO)_2C_6H_9O_3$ (bi-methoxy capped glucopyraonse monomer unit).

Reaction	ΔG_r /kcal mol^{-1}			
	ωB97X-D	PCM	B3LYP	PCM
$N_2O_4 + H_2O \longrightarrow HNO_3 + HNO_2$	2.25	1.85	5.13	4.18
$N_2O_4 \rightleftharpoons 2\,^{\cdot}NO_2$	0.12	1.46	−0.54	−0.16
Radical reactions				
$^{\cdot}NO_2 + HNO \longrightarrow HNO_2 + {}^{\cdot}NO$	−28.22	−28.67	−27.33	−27.63
$2\,^{\cdot}NO + O_2 \longrightarrow 2\,^{\cdot}NO_2$	−20.77	−21.97	−21.16	−22.16
Acid reactions				
$HNO_3 + HNO_2 \rightleftharpoons N_2O_4 + H_2O$	−2.25	−1.85	−5.13	−4.18
$4\,HNO_3 \rightleftharpoons 4\,^{\cdot}NO_2 + 2\,H_2O + O_2$	53.35	58.36	42.61	46.94
$2\,HNO \longrightarrow HON{=}NOH$	−38.97	−39.72	−36.63	−37.41
$HON{=}NOH \longrightarrow N_2O + H_2O$	−48.08	−48.18	−50.55	−50.75
Ionic reactions				
$NO_2^+ + 2\,H_2O \rightleftharpoons HNO_3 + H_3O^+$	−0.90	−1.34	1.77	2.46
EN (R = CH_3CH_2)				
$R{-}ONO_2 + H_2O \longrightarrow R{-}OH + HNO_3$	4.56	5.24	4.00	4.86
$R{-}OH + HNO_3 \longrightarrow R{=}O + HNO_2 + H_2O$	−34.06	−38.43	−37.59	−41.77
$R{-}OH + {}^{\cdot}NO_2 \longrightarrow {}^{\cdot}R{-}OH + HNO_2$	16.38	13.92	15.89	13.70
$^{\cdot}R{-}OH + HNO_3 \longrightarrow R{=}O + H_2O + {}^{\cdot}NO_2$	−50.44	−52.35	−53.48	−55.47
$R{-}OH + HNO_2 \rightleftharpoons R{-}ONO + H_2O$	−3.21	−3.28	−2.64	−2.95
$R{-}ONO \longrightarrow R{=}O + HNO$	−1.50	−5.82	−4.37	−8.50
NC monomer (R = $(H_3CO)_2C_6H_9O_3$)				
$R{-}ONO_2 + H_2O \longrightarrow R{-}OH + HNO_3$	0.68	5.63	0.61	−0.70
$R{-}OH + HNO_3 \longrightarrow R{=}O + HNO_2 + H_2O$	−36.73	−38.34	−41.71	−41.70
$R{-}OH + {}^{\cdot}NO_2 \longrightarrow {}^{\cdot}R{-}OH + HNO_2$	14.71	11.15	13.03	23.21
$^{\cdot}R{-}OH + HNO_3 \longrightarrow R{=}O + H_2O + {}^{\cdot}NO_2$	−51.44	−49.49	−54.75	−56.37
$R{-}OH + HNO_2 \rightleftharpoons R{-}ONO + H_2O$	−4.43	−7.30	−4.31	−0.18
$R{-}ONO \longrightarrow R{=}O + HNO$	−2.93	−1.71	−6.82	−11.21

that it is the NO_2 species driving oxidation in all three schemes, and plays a central role in the extended degradation scheme of NC.

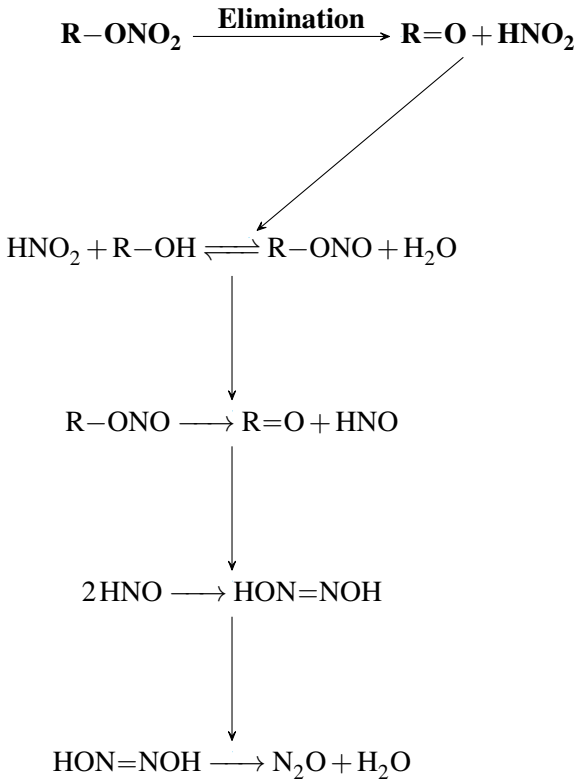

Scheme 1.6: Proposed degradation pathway starting from the elimination of HNO_2 from a nitrate ester, derived from the schemes presented by Camera [4] and Aellig[6].

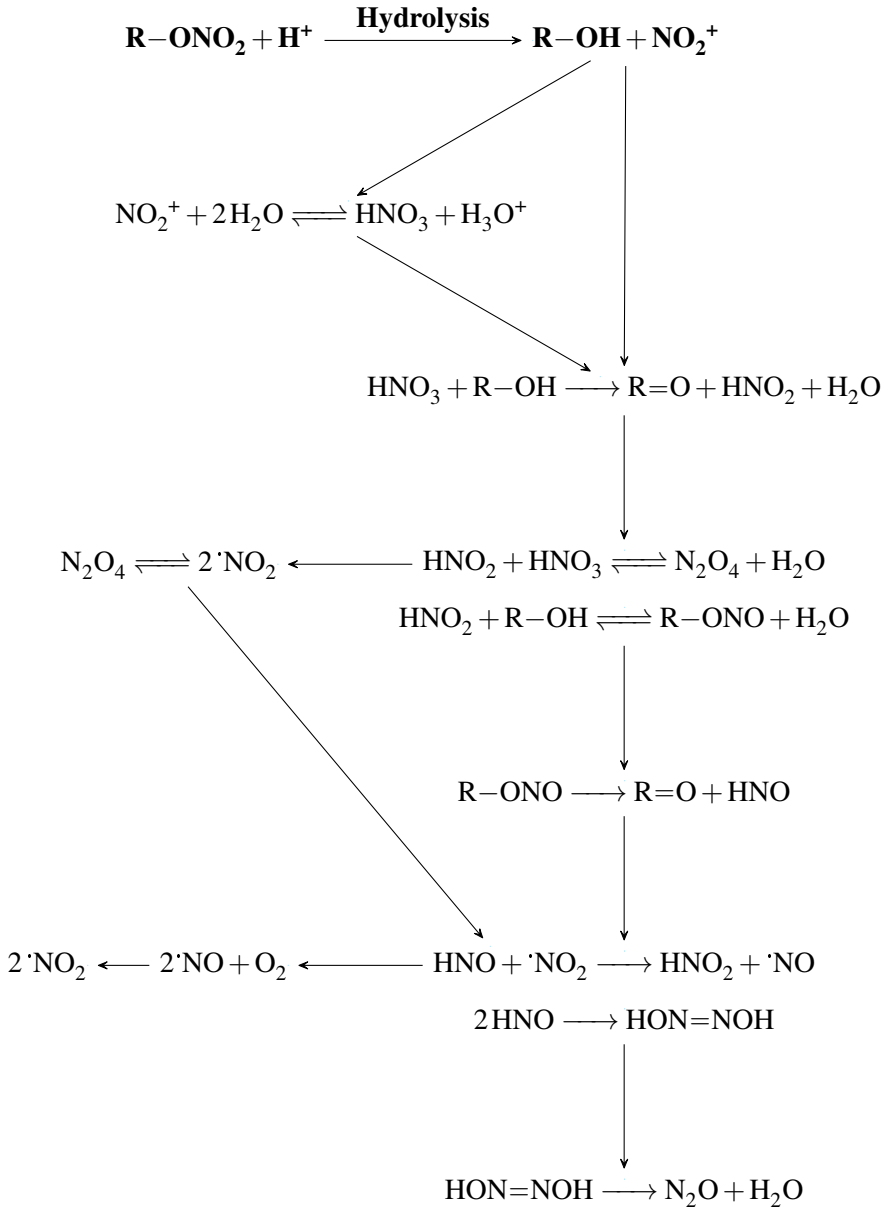

Scheme 1.7: Proposed degradation pathway starting from the acid hydrolysis of a nitrate ester, derived from the schemes presented by Camera [4] and Aellig[6].

Bibliography

[1] Manoj K Shukla and Frances Hill. Computational elucidation of mechanisms of alkaline hydrolysis of nitrocellulose: dimer and trimer models with comparison to the corresponding monomer. *The journal of physical chemistry. A*, 116(29):7746–55, 2012.

[2] Roman V. Tsyshevsky, Onise Sharia, and Maija M. Kuklja. Thermal Decomposition Mechanisms of Nitroesters: Ab Initio Modeling of Pentaerythritol Tetranitrate. *The Journal of Physical Chemistry C*, 117(35):18144–18153, sep 2013.

[3] Mohammed Moniruzzaman, John M. Bellerby, and Manfred A. Bohn. Activation energies for the decomposition of nitrate ester groups at the anhydroglucopyranose ring positions C2, C3 and C6 of nitrocellulose using the nitration of a dye as probe. *Polymer Degradation and Stability*, 102:49–58, apr 2014.

[4] E. Camera, G. Modena, and B. Zotti. On the Behaviour of Nitrate Esters in Acid Solution. II. Hydrolysis and oxidation of nitroglycol and nitroglycerin. *Propellants, Explosives, Pyrotechnics*, 7(3):66–69, jun 1982.

[5] Anton Chin, Daniel S. Ellison, Sara K. Poehlein, and Myong K. Ahn. Investigation of the Decomposition Mechanism and Thermal Stability of Nitrocellulose/Nitroglycerine Based Propellants by Electron Spin Resonance. *Propellants, Explosives, Pyrotechnics*, 32(2):117–126, apr 2007.

[6] Christof Aellig, Christophe Girard, and Ive Hermans. Aerobe Alkoholoxidation mithilfe von HNO3. *Angewandte Chemie*, 123(51):12563–12568, dec 2011.

[7] K. S. Hu, A. I. Darer, and M. J. Elrod. Thermodynamics and kinetics of the hydrolysis of atmospherically relevant organonitrates and organosulfates. *Atmospheric Chemistry and Physics*, 11(16):8307–8320, aug 2011.

[8] M. Moniruzzaman and J.M. Bellerby. Use of UV visible spectroscopy to monitor nitrocellulose degradation in thin films. *Polymer Degradation and Stability*, 93(6):1067–1072, jun 2008.

[9] T. Shepodd, R. Behrens, D. Anex, D. Miller, and K. Anderson. Degradation chemistry of PETN and its homologues. Technical report, Sandia National Laboratories (SNL), Albuquerque, NM, and Livermore, CA (United States), nov 1997.

[10] Fotis Rigas, Ioannis Sebos, and Danae Doulia. Safety Charts Simulation of Nitroglycerine/Nitroglycol Spent Acids via Chemical Reaction Kinetics. *Industrial and Engineering Chemistry Research*, 36(12):5068–5073, 1997.

[11] S. J. Buelow, D. Allen, G. K. Anderson, F. L. Archuleta, and J. H. Atencio. Destruction of Energetic Materials in Supercritical Water. Technical report, AIR FORCE RESEARCH LABORATORY, 2002.

[12] L. Dauerman and Y. A. Tajima. Thermal decomposition and combustion of nitrocellulose. *AIAA Journal*, 6(8):1468–1473, aug 1968.

[13] John W. Baker and D. M. Easty. Hydrolytic decomposition of esters of nitric acid. Part I. General experimental techniques. Alkaline hydrolysis and neutral solvolysis of methyl, ethyl, isopropyl, and tert.-butyl nitrates in aqueous alcohol. *Journal of the Chemical Society (Resumed)*, 1952(0):1193–1207, 1952.

[14] E. Camera, G. Modena, and B. Zotti. On the behaviour of nitrate esters in acid solution. III. Oxidation of ethanol by nitric acid in sulphuric acid. *Propellants, Explosives, Pyrotechnics*, 8(3):70–73, jun 1983.

[15] V. G. Matveev and G. M. Nazin. Stepwise Degradation of Polyfunctional Compounds. *Kinetics and Catalysis*, 44(6):735–739, nov 2003.

[16] Juan F. Arenas, Francisco J. Avila, Juan C. Otero, Daniel Peláez, Juan Soto, and Juan Soto. Approach to the atmospheric chemistry of methyl nitrate and methylperoxy nitrite. Chemical mechanisms of their formation and decomposition reactions in the gas phase. *Journal of Physical Chemistry A*, 112(2):249–255, 2007.

[17] Frank E. Wolf. Alkaline Hydrolyis Conversion of Nitrocellulose Fines. Technical Report October, Badger Army Ammunition Plant, oct 1997.

[18] Russell D. Johnson III. NIST Computational Chemistry Comparison and Benchmark Database NIST Standard Reference Database Number 101, 2018.

[19] I. Rodger and J. D. Mcirvine. The decomposition of spent PETN nitration acids. *The Canadian Journal of Chemical Engineering*, 41(2):87–90, apr 1963.

[20] Torbjórn Lindblom. Reactions in stabilizer and between stabilizer and nitrocellulose in propellants. *Propellants, Explosives, Pyrotechnics*, 27(4):197–208, sep 2002.

[21] Hermann N. Volltrauer and Arthur Fontijn. Low-temperature pyrolysis studies by chemiluminescence techniques real-time nitrocellulose and PBX 9404 decomposition. *Combustion and Flame*, 41(C):313–324, jan 1981.

[22] Neha Awasthi, Thomas Ritschel, Reinhard Lipowsky, and Volker Knecht. Standard Gibbs energies of formation and equilibrium constants from ab-initio calculations: Covalent dimerization of NO2 and synthesis of NH3. *Journal of Chemical Thermodynamics*, 62:211–221, jul 2013.

[23] H. K. Roscoe and A. K. Hind. The equilibrium constant of NO2 with N2O4 and the temperature dependence of the visible spectrum of NO2: A critical review and the implications for measurements of NO2 in the polar stratosphere. *Journal of Atmospheric Chemistry*, 16(3):257–276, apr 1993.